



Crystal structure of oxibendazole, C₁₂H₁₅N₃O₃James A. Kaduk ^{1,2,a)} Stacy Gates-Rector ³ and Thomas N. Blanton ³¹Illinois Institute of Technology, 3101 S. Dearborn St., Chicago, IL 60616, USA²North Central College, 131 S. Loomis St., Naperville, IL 60540, USA³ICDD, 12 Campus Blvd., Newtown Square, PA 19073-3273, USA

(Received 31 August 2022; accepted 26 September 2022)

The crystal structure of oxibendazole has been solved and refined using synchrotron X-ray powder diffraction data, and optimized using density functional theory techniques. Oxibendazole crystallizes in space group *C2/c* (#15) with $a = 23.18673(22)$, $b = 5.35136(5)$, $c = 19.88932(13)$ Å, $\beta = 97.0876(9)^\circ$, $V = 2449.018(17)$ Å³, and $Z = 8$. The structure consists of hydrogen-bonded layers of planar molecules parallel to the *bc*-plane. Strong N–H⋯N hydrogen bonds link the molecules into dimers, with a graph set R2,2(8). N–H⋯O hydrogen bonds further link these dimers into layers parallel to the *bc*-plane. The powder pattern has been submitted to ICDD for inclusion in the Powder Diffraction File™ (PDF®).

© The Author(s), 2023. Published by Cambridge University Press on behalf of International Centre for Diffraction Data. This is an Open Access article, distributed under the terms of the Creative Commons Attribution licence (<http://creativecommons.org/licenses/by/4.0/>), which permits unrestricted re-use, distribution and reproduction, provided the original article is properly cited.

[doi:10.1017/S0885715622000495]

Key words: oxibendazole, Loditac, powder diffraction, Rietveld refinement, density functional theory

I. INTRODUCTION

Oxibendazole (sold under the brand name Loditac among others) is used to protect against roundworms, threadworms, pinworms, and lungworm infestations in horses and some domestic pets. The systematic name (CAS Registry Number 20559-55-1) is methyl *N*-(6-propoxy-1H-benzimidazol-2-yl) carbamate. A two-dimensional molecular diagram is shown in Figure 1. As is the case with some other veterinary pharmaceuticals, we are unaware of any published X-ray powder diffraction data for this compound.

This work was carried out as part of a project (Kaduk *et al.*, 2014) to determine the crystal structures of large-volume commercial pharmaceuticals, and include high-quality powder diffraction data for them in the Powder Diffraction File (Gates-Rector and Blanton, 2019).

II. EXPERIMENTAL AND REFINEMENT

Oxibendazole was a commercial reagent, purchased from TargetMol (Batch #143644), and was used as-received. The white/cream powder was packed into a 1.5 mm diameter Kapton capillary and rotated during the measurement at ~50 Hz. The powder pattern was measured at 295 K at beamline 11-BM (Antao *et al.*, 2008; Lee *et al.*, 2008; Wang *et al.*, 2008) of the Advanced Photon Source at Argonne National Laboratory using a wavelength of 0.458200(2) Å from 0.5 to 50° 2θ with a step size of 0.001°, and a counting time of 0.1 s step⁻¹. The high-resolution powder diffraction data were collected using twelve silicon crystal analyzers that

allow for high angular resolution, high precision, and accurate peak positions. A mixture of silicon (NIST SRM 640c) and alumina (NIST SRM 676a) standards (ratio Al₂O₃:Si = 2:1 by weight) was used to calibrate the instrument and refine the monochromatic wavelength used in the experiment.

The pattern was difficult to index, but a reasonable unit cell (volume corresponding to an integral number of molecules) was obtained using N-TREOR (Altomare *et al.*, 2013). A monoclinic cell with $a = 23.199$, $b = 5.3497$, $c = 19.8957$ Å, $\beta = 97.061^\circ$, $V = 2450.5$ Å³, and $Z = 8$ was obtained. The systematic absences corresponded to space groups *Cc* or *C2/c*. Since the volume of the unit cell corresponded to 8 molecules, space group *C2/c* was assumed, and confirmed by successful solution and refinement of the structure. A reduced cell search in the Cambridge Structural Database (Groom *et al.*, 2016) yielded no hits. A few weak

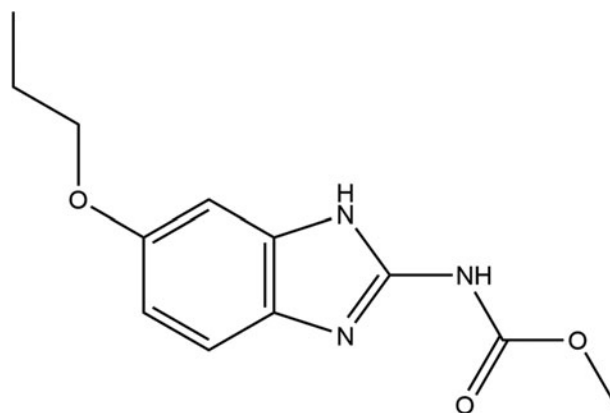


Figure 1. The 2D molecular structure of oxibendazole.

^{a)} Author to whom correspondence should be addressed. Electronic mail: kaduk@polycrystallography.com

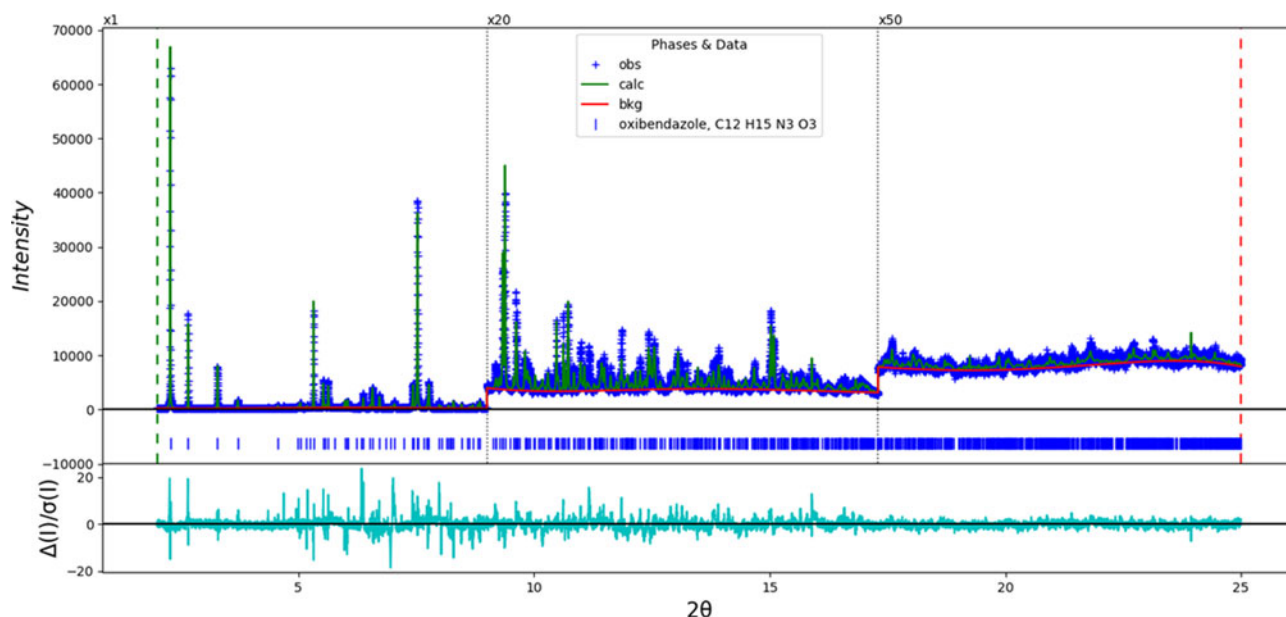


Figure 2. The Rietveld plot for the refinement of oxibendazole. The blue crosses represent the observed data points, and the green line is the calculated pattern. The cyan curve is the normalized error plot, and the red line is the background curve. The vertical scale has been multiplied by a factor of 20 \times for $2\theta > 9.0^\circ$, and by 50 \times for $2\theta > 17.3^\circ$. The row of blue tick marks indicates the calculated reflection positions of oxibendazole.

(<0.5% relative intensity) were not indexed by this cell, so the sample seems to contain at least one impurity phase.

An oxibendazole molecule was downloaded as Conformer3D_CID_4622.sdf from PubChem (Kim *et al.*, 2019). The file was converted to a *.mol2 file using Mercury (Macrae *et al.*, 2020). The structure was solved using Monte Carlo simulated annealing techniques as implemented in DASH (David *et al.*, 2006), including a (010) preferred orientation coefficient. Seven of the 100 runs yielded cost factors much lower than the others. The best solution was selected for refinement. Equivalent solutions were also obtained using EXPO2014 (Altomare *et al.*, 2013).

Rietveld refinement was carried out using GSAS-II (Toby and Von Dreele, 2013). Only the 2.0–25.0 $^\circ$ portion of the pattern was included in the refinement ($d_{\min} = 1.058 \text{ \AA}$). All non-H bond distances and angles were subjected to restraints, based on a Mercury/Mogul Geometry Check (Bruno *et al.*, 2004; Sykes *et al.*, 2011). The Mogul average and standard deviation for each quantity were used as the restraint parameters, but the standard deviations of the bond distances and angles in the propoxy side chain were decreased to 0.03 \AA and 3.0 $^\circ$. The restraints contributed 9.0% to the final χ^2 .

The initial model contained a small void on a twofold axis at approximately 0,0.24,1/4. Including an oxygen atom (water molecule) at this position resulted in a negative occupancy, so the atom was removed. The U_{iso} of the atoms in the propoxy side chain refined to very large values ($>0.3 \text{ \AA}^2$), suggesting the possibility of disorder. The propoxy chain was thus modeled as a superposition of two orientations. The occupancies refined to 51/49%. The hydrogen atoms were included in calculated positions, which were recalculated during the refinement using Materials Studio (Dassault, 2021). The U_{iso} of the heavy atoms were grouped by chemical similarity. The U_{iso} for the H atoms were fixed at 1.3 \times the U_{iso} of the heavy atoms to which they are attached. A fourth-order spherical harmonic model was included in the refinement. The refined texture index was 1.044(1). The peak profiles were described using the Stephens (1999) generalized microstrain model. Initial refinements used a uniaxial (010) microstrain model. When the microstrain model was switched to generalized, the residuals decreased, but the refinement eventually diverged (even using a Jacobian rather than a Hessian least squares matrix). In the final refinement, the S_{hkl} coefficients were fixed at the values which yielded the best fit before

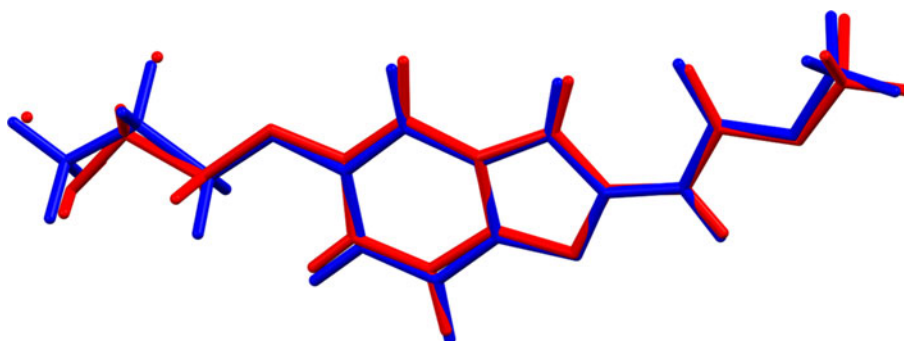


Figure 3. Comparison of the Rietveld-refined (red) and VASP-optimized (blue) structures of oxibendazole. The rms Cartesian displacement is 0.217 \AA . Image generated using Mercury (Macrae *et al.*, 2020).

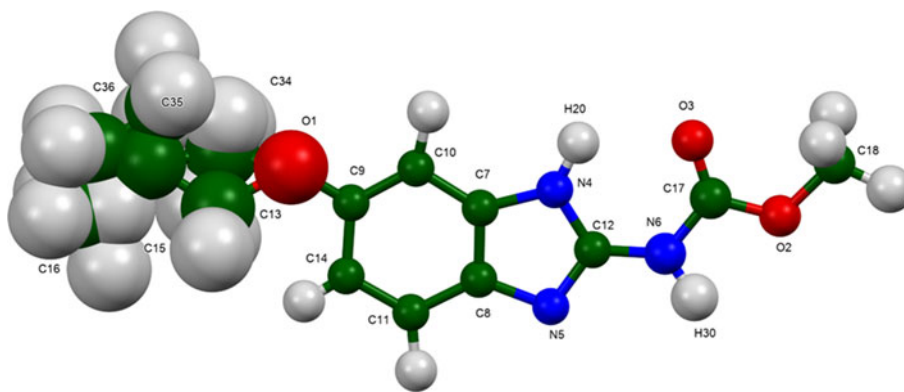


Figure 4. The asymmetric unit of oxibendazole, with the atom numbering. The atoms are represented by 50% probability spheroids/ellipsoids. Image generated using Mercury (Macrae *et al.*, 2020).

divergence. The background was modeled using a 6-term shifted Chebyshev polynomial, and a peak at $5.48^\circ 2\theta$ to model the scattering from the Kapton capillary and any amorphous component.

The final refinement of 86 variables using 23 037 observations and 51 restraints yielded the residuals $R_{wp} = 0.1291$ and $GOF = 2.47$. The largest peak (1.19 \AA from C14) and hole (1.62 \AA from N4) in the difference Fourier map were 0.64 (13) and -0.55 (13) $e\text{\AA}^{-3}$, respectively. The largest errors in the difference plot (Figure 2) are in the shapes and intensities of some of the strong low-angle peaks, and reflect the imperfect profile model and the impurity peaks.

The crystal structure of an ordered model of oxibendazole, with one orientation of the propoxy side chain, was optimized using VASP (Kresse and Furthmüller, 1996) (fixed experimental unit cell) through the MedeA graphical interface (Materials Design, 2016). The calculation was carried out on 16 2.4 GHz processors (each with 4 GB RAM) of a

64-processor HP Proliant DL580 Generation 7 Linux cluster at North Central College. The calculation used the GGA-PBE functional, a plane wave cutoff energy of 400.0 eV, and a k -point spacing of 0.5 \AA^{-1} leading to a $5 \times 1 \times 5$ mesh, and took ~ 44 h. A single-point density functional theory calculation (fixed experimental cell) and population analysis were carried out using CRYSTAL17 (Dovesi *et al.*, 2018). The basis sets for the H, C, N, and O atoms in the calculation were those of Gatti *et al.* (1994). The calculations were run on a 3.5 GHz PC using 8 k -points and the B3LYP functional, and took ~ 1.5 h.

III. RESULTS AND DISCUSSION

The root-mean-square (rms) Cartesian displacement between the Rietveld-refined and DFT-optimized structures of the oxibendazole molecule is 0.217 \AA (Figure 3); the maximum difference is 0.569 \AA at the methyl group C16 at the end

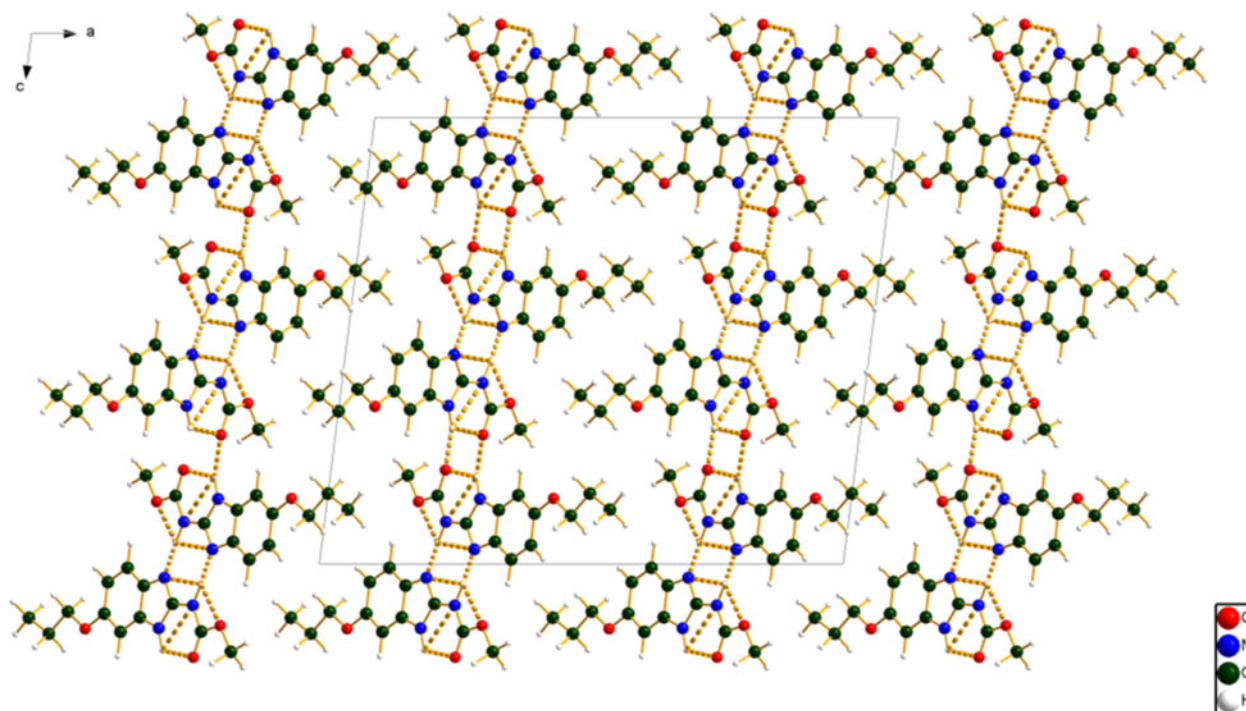


Figure 5. The crystal structure of oxibendazole, viewed down the b -axis. Image generated using Diamond (Crystal Impact, 2022).

TABLE I. Hydrogen bonds (CRYSTAL17) in oxibendazole.

H-Bond	D-H (Å)	H...A (Å)	D...A (Å)	D-H...A (°)	Overlap (e)	E (kcal mol ⁻¹)
N6-H30...N5	1.076	1.697	2.772	175.4	0.106	
N4-H20...O3	1.022	2.146	2.952	134.3	0.029	3.9
C11-H21...O2	1.089	2.465	3.397	142.9	0.012	
C10-H19...O3	1.088	2.568	3.294	123.4	0.011	

of the propoxy chain. The agreement is within the normal range for correct structures (van de Streek and Neumann, 2014). Because the DFT optimization required an ordered structure, only one of the two orientations of the propoxy chain was used (the one with the lower atom numbers: C13, C15, and C16). The apparent void in the experimental structure disappeared on DFT optimization. The void was located near the propoxy chains and may provide a reason for the apparent disorder. This discussion concentrates on the DFT-optimized structure. The asymmetric unit (with atom numbering) is illustrated in Figure 4. The displacement coefficients of the disordered chain are much larger than those in the rest of the molecule, consistent with the disorder. The best view of the crystal structure is down the short *b*-axis (Figure 5). The structure consists of hydrogen-bonded layers of planar molecules parallel to the *bc*-plane. The propoxy groups lie on the outer surfaces of the layers. The mean planes of the benzimidazole ring systems are approximately (510) and (5-10). The Aromatics Analyser module of Mercury indicates only two moderate-strength interactions; one of 5.35 Å along the *b*-axis, and the other of 6.60 Å within the hydrogen-bonded layers.

All of the bond distances, bond angles, and torsion angles fall within the normal ranges indicated by a Mercury/Mogul Geometry Check (Macrae *et al.*, 2020). Quantum chemical geometry optimization of the isolated oxibendazole molecule (DFT/B3LYP/6-31G*/water) using Spartan '18 (Wavefunction, 2020) indicated that the observed conformation of the first orientation (lower atom numbers) is the minimum-energy conformation. Both orientations of the propoxy group converged to

the same local minimum. The relatively-loose packing of the propoxy groups (few short contacts) is consistent with the apparent disorder of these groups.

Analysis of the contributions to the total crystal energy of the structure using the Forcite module of Materials Studio (Dassault, 2021) suggests that the intramolecular deformation energy is dominated by angle deformation terms, as expected for a fused ring system. The intermolecular energy is dominated by van der Waals and electrostatic attractions, which in this force field analysis also include hydrogen bonds. The hydrogen bonds are better analyzed using the results of the DFT calculation.

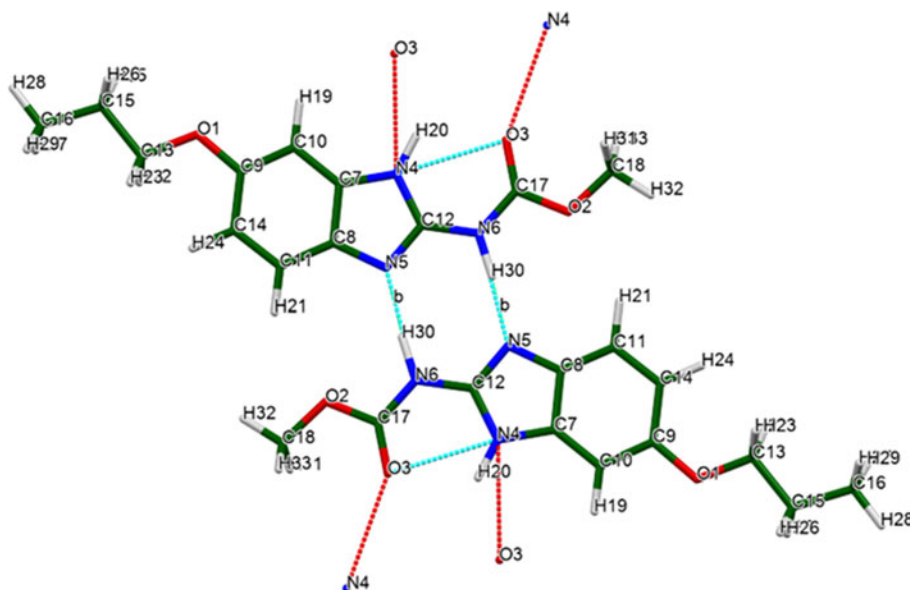
Hydrogen bonds are prominent in the structure (Table I). Strong N6-H30...N5 hydrogen bonds link the molecules into dimers (Figure 6), with a graph set (Etter, 1990; Bernstein *et al.*, 1995; Shields *et al.*, 2000) *R2,2(8)*. N4-H20...O3 hydrogen bonds further link these dimers into layers parallel to the *bc*-plane. The energy of the N-H...O hydrogen bond was calculated using the correlation of Wheatley and Kaduk (2019). C-H...O hydrogen bonds also contribute to the lattice energy.

The volume enclosed by the Hirshfeld surface of oxibendazole (Figure 7; Spackman *et al.*, 2021) is 299.30 Å³, 97.77% of 1/8 the unit cell volume. The packing density is thus fairly typical. The only significant close contacts (red in Figure 7) involve the hydrogen bonds. The average volume/non-hydrogen atom is 17.0 Å³.

The Bravais-Friedel-Donnay-Harker (Bravais, 1866; Friedel, 1907; Donnay and Harker, 1937) morphology suggests that we might expect elongated morphology for oxibendazole, with [010] as the unique axis. A fourth-order spherical harmonic model was included in the refinement. The texture index was 1.044(1), indicating that preferred orientation was small in this rotated capillary specimen.

IV. DEPOSITED DATA

The powder pattern of oxibendazole from this synchrotron data set has been submitted to ICDD for inclusion in the Powder Diffraction File. The Crystallographic

Figure 6. The oxibendazole dimers, generated by the strong N-H...N hydrogen bonds. Image generated using Mercury (Macrae *et al.*, 2020).

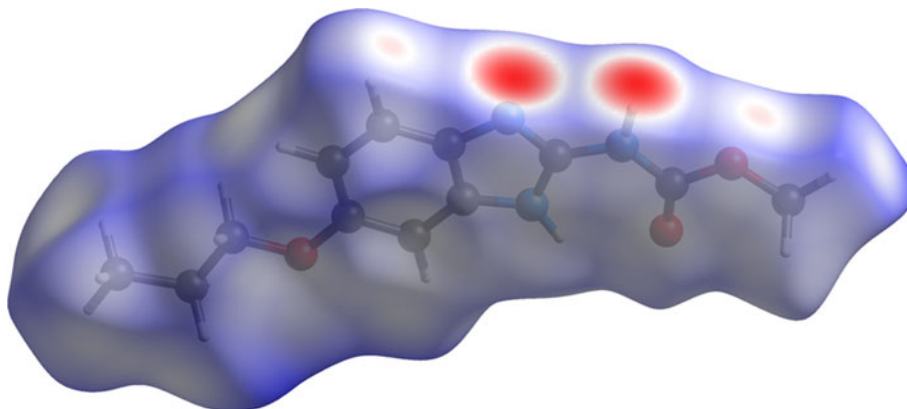


Figure 7. The Hirshfeld surface of oxibendazole. Intermolecular contacts longer than the sums of the van der Waals radii are colored blue, and contacts shorter than the sums of the radii are colored red. Contacts equal to the sums of radii are white. Image generated by CrystalExplorer 21.5 (Spackman *et al.*, 2021).

Information Framework (CIF) files containing the results of the Rietveld refinement (including the raw data) and the DFT geometry optimization were deposited with the ICDD. The data can be requested at pdj@icdd.com.

ACKNOWLEDGEMENTS

The use of the Advanced Photon Source at Argonne National Laboratory was supported by the U.S. Department of Energy, Office of Science, Office of Basic Energy Sciences, under Contract No. DE-AC02-06CH11357. This work was partially supported by the International Centre for Diffraction Data. We thank Lynn Ribaud and Saul Lapidus for their assistance in the data collection.

CONFLICT OF INTEREST

The authors have no conflict of interest to declare.

REFERENCES

- Altomare, Angela, Corrado Cuocci, Carmelo Giacobozzo, Anna Moliterni, Rosanna Rizzi, Nicola Corriero, and Aurelia Falcicchio. 2013. "EXPO2013: A Kit of Tools for Phasing Crystal Structures from Powder Data." *Journal of Applied Crystallography* 46 (4): 1231–5.
- Antao, Sytle M., Ishmael Hassan, Jun Wang, Peter L. Lee, and Brian H. Toby. 2008. "State-of-the-Art High-Resolution Powder X-Ray Diffraction (HRPXRD) Illustrated with Rietveld Structure Refinement of Quartz, Sodalite, Tremolite, and Meionite." *The Canadian Mineralogist* 46 (6): 1501–9.
- Bernstein, Joel, Raymond E. Davis, Liat Shimoni, and Ning-Leh Chang. 1995. "Patterns in Hydrogen Bonding: Functionality and Graph Set Analysis in Crystals." *Angewandte Chemie International Edition in English* 34 (15): 1555–73.
- Bravais, Auguste. 1866. *Etudes Cristallographiques*. Paris, Gauthier-Villars.
- Bruno, Ian J., Jason C. Cole, Magnus Kessler, Jie Luo, WD Sam Motherwell, Lucy H. Purkis, Barry R. Smith, Robin Taylor, Richard I. Cooper, Stephanie E. Harris, and A. Guy Orpen. 2004. "Retrieval of Crystallographically-Derived Molecular Geometry Information." *Journal of Chemical Information and Computer Sciences* 44 (6): 2133–44.
- Dassault Systèmes. 2021. *Materials Studio 2021*. San Diego, CA, BIOVIA.
- David, William IF, Kenneth Shankland, Jacco Van De Streek, Elna Pidcock, WD Samuel Motherwell, and Jason C. Cole. 2006. "DASH: A Program for Crystal Structure Determination from Powder Diffraction Data." *Journal of Applied Crystallography* 39 (6): 910–5.
- Donnay, J. D H., and David Harker. 1937. "A New Law of Crystal Morphology Extending the Law of Bravais." *American Mineralogist: Journal of Earth and Planetary Materials* 22 (5): 446–67.
- Dovesi, Roberto, Alessandro Erba, Roberto Orlando, Claudio M. Zicovich-Wilson, Bartolomeo Civalleri, Lorenzo Maschio, Michel Rérat, Silvia Casassa, Jacopo Baima, Simone Salustro, and Bernard Kirtman. 2018. "Quantum-Mechanical Condensed Matter Simulations with CRYSTAL." *Wiley Interdisciplinary Reviews: Computational Molecular Science* 8 (4): e1360.
- Etter, Margaret C. 1990. "Encoding and Decoding Hydrogen-Bond Patterns of Organic Compounds." *Accounts of Chemical Research* 23 (4): 120–6.
- Friedel, Georges. 1907. "Etudes sur la loi de Bravais." *Bulletin de Minéralogie* 30 (9): 326–455.
- Gates-Rector, Stacy, and Thomas Blanton. 2019. "The Powder Diffraction File: A Quality Materials Characterization Database." *Powder Diffraction* 34 (4): 352–60.
- Gatti, C., V. R. Saunders, and C. Roetti. 1994. "Crystal Field Effects on the Topological Properties of the Electron Density in Molecular Crystals: The Case of Urea." *The Journal of Chemical Physics* 101 (12): 10686–96.
- Groom, C. R., Bruno, I. J., Lightfoot, M. P., and Ward, S. C. 2016. "The Cambridge Structural Database." *Acta Crystallographica Section B. Structural Science, Crystal Engineering and Materials* 72, 171–9.
- Kaduk, James A., Cyrus E. Crowder, Kai Zhong, Timothy G. Fawcett, and Matthew R. Suchoemel. 2014. "Crystal Structure of Atomoxetine Hydrochloride (Strattera), C₁₇H₂₂NOCl." *Powder Diffraction* 29 (3): 269–73.
- Kim, Sunghwan, Jie Chen, Tiejun Cheng, Asta Gindulyte, Jia He, Siqian He, Qingliang Li, Benjamin A. Shoemaker, Paul A. Thiessen, Bo Yu, Leonid Zaslavsky, Jian Zhang, and Evan E. Bolton. 2019. "PubChem 2019 Update: Improved Access to Chemical Data." *Nucleic Acids Research* 47 (D1): D1102–9. doi:10.1093/nar/gky1033.
- Kresse, Georg, and Jürgen Furthmüller. 1996. "Efficiency of ab-initio Total Energy Calculations for Metals and Semiconductors Using a Plane-Wave Basis Set." *Computational Materials Science* 6 (1): 15–50.
- Lee, Peter L., Deming Shu, Mohan Ramanathan, Curt Preissner, Jun Wang, Mark A. Beno, Robert B. Von Dreele, Lynn Ribaud, Charles Kurtz, Sytle M. Antao, Xuesong Jiao, and Brian H. Toby. 2008. "A Twelve-Analyzer Detector System for High-Resolution Powder Diffraction." *Journal of Synchrotron Radiation* 15 (5): 427–32.
- Macrae, Clare F., Ioana Sovago, Simon J. Cottrell, Peter T. A. Galek, Patrick McCabe, Elna Pidcock, Michael Platings, Greg P. Shields, Joanna S. Stevens, Matthew Towler, and Peter A. Wood. 2020. "Mercury 4.0: From Visualization to Analysis, Design and Prediction." *Journal of Applied Crystallography* 53 (1): 226–35.
- Materials Design. 2016. *MedeA 2.20.4*. Angel Fire, NM, Materials Design Inc.
- Putz, Crystal Impact-Dr H., and Dr K. Brandenburg. 2022. "Diamond-Crystal and Molecular Structure Visualization. Kreuzherrenstr. 102, 53227 Bonn, Germany." <https://www.crystalimpact.de/diamond>.
- Shields, Gregory P., Paul R. Raithby, Frank H. Allen, and WD Samuel Motherwell. 2000. "The Assignment and Validation of Metal Oxidation States in the Cambridge Structural Database." *Acta Crystallographica Section B: Structural Science* 56 (3): 455–65.

- Spackman, Peter R., Michael J. Turner, Joshua J. McKinnon, Stephen K. Wolff, Daniel J. Grimwood, Dylan Jayatilaka, and Mark A. Spackman. 2021. "CrystalExplorer: A Program for Hirshfeld Surface Analysis, Visualization and Quantitative Analysis of Molecular Crystals." *Journal of Applied Crystallography* 54 (3): 1006–11.
- Stephens, Peter W. 1999. "Phenomenological Model of Anisotropic Peak Broadening in Powder Diffraction." *Journal of Applied Crystallography* 32 (2): 281–9.
- Sykes, Richard A., Patrick McCabe, Frank H. Allen, Gary M. Battle, Ian J. Bruno, and Peter A. Wood. 2011. "New Software for Statistical Analysis of Cambridge Structural Database Data." *Journal of Applied Crystallography* 44 (4): 882–6.
- Toby, Brian H., and Robert B. Von Dreele. 2013. "GSAS-II: The Genesis of a Modern Open-Source all Purpose Crystallography Software Package." *Journal of Applied Crystallography* 46 (2): 544–9.
- van de Streek, Jacco, and Marcus A. Neumann. 2014. "Validation of Molecular Crystal Structures from Powder Diffraction Data with Dispersion-Corrected Density Functional Theory (DFT-D)." *Acta Crystallographica. Section B, Structural Science, Crystal Engineering and Materials* 70 (Pt 6): 1020–32.
- Wang, Jun, Brian H. Toby, Peter L. Lee, Lynn Ribaud, Sytle M. Antao, Charles Kurtz, Mohan Ramanathan, Robert B. Von Dreele, and Mark A. Beno. 2008. "A Dedicated Powder Diffraction Beamline at the Advanced Photon Source: Commissioning and Early Operational Results." *Review of Scientific Instruments* 79 (8): 085105.
- Wavefunction, Inc. 2020. "Spartan '18" Version 1.4.5. Irvine, CA, Wavefunction, Inc.
- Wheatley, Austin M., and James A. Kaduk. 2019. "Crystal Structures of Ammonium Citrates." *Powder Diffraction* 34 (1): 35–43.